Crystals **2012**, *2*, 1-21; doi: 10.3390/cryst2010001

OPEN ACCESS

crystals

ISSN 2073-4352

www.mdpi.com/journal/crystals

Article

Differential Scanning Calorimetry (DSC) and Synchrotron X-ray Diffraction Study of Unmilled and Milled $LiBH_4$: A Partial Release of Hydrogen at Moderate Temperatures

J. Lang [1], A. Gerhauser [2], Y. Filinchuk [3,4,*], T. Klassen [2] and J. Huot [1,*]

[1] Hydrogen Research Institute, Université du Québec à Trois-Rivières, 3351 Boul. des Forges, Trois-Rivières, Québec, G9A 5H7, Canada

[2] Institute of Materials Technology, Helmut-Schmidt-University, Holstenhofweg 85, D-22043 Hamburg, Germany

[3] Swiss-Norwegian Beam Lines at ESRF, BP-220, 38043 Grenoble, France

[4] Institute of Condensed Matter and Nanosciences, Université Catholique de Louvain, B-1348 Louvain-la-Neuve, Belgium

* Authors to whom correspondence should be addressed; E-Mails: yaroslav.filinchuk@uclouvain.be (Y.F.); jacques.huot@uqtr.ca (J.H.); Fax: +32-10-47-27-07 (Y.F.); +1-819-376-5164 (J.H.).

Received: 30 September 2011; in revised form: 9 December 2011 / Accepted: 14 December 2011 / Published: 27 December 2011

Abstract: A systematic investigation of phase transitions in unmilled and milled $LiBH_4$ has been performed by Pressurized Differential Scanning Calorimetry (PDSC). It was found that a large exotherm is present below the low temperature (LT) → high temperature (HT) phase transition. This exotherm is not caused by air contamination but seems to originate from hydrogen release from a solid solution in the matrix of $LiBH_4$ low temperature phase. The exotherm activation energy has been measured to be 100 kJ mol^{-1}. Calorimetric measurements under argon and hydrogen have shown that for the milled sample, the endothermic peak of the LT → HT transition is split in two when the PDSC scan is performed under hydrogen atmosphere. Synchrotron X-ray powder diffraction on the milled $LiBH_4$ sample revealed only a single-step transition from the LT to HT phase, both under vacuum and under 2 and 40 bar of hydrogen pressure. The axial ratios for the LT $LiBH_4$ below 300 K are significantly altered by milling; they are also considerably different under 40 bar of hydrogen, indicating an interaction between the hydrogen gas and the LT $LiBH_4$ solid phase.

Keywords: hydrogen storage materials; complex hydrides; Pressure DSC; phase transition; synchrotron X-ray diffraction

1. Introduction

In the perspective of a future hydrogen economy, there is an obvious need for hydrogen storage material that has high volumetric and gravimetric capacity as well as low cost and low temperature of operation. In this respect, the potential of lithium boro-hydride $LiBH_4$ as hydrogen storage material has been recently exposed by Züttel *et al.* [1]. The reaction has an enthalpy of formation of –74 kJ mol^{-1} and a hydrogen capacity of 13.8 wt% [2]. As this hydrogen reaction enthalpy is comparable to magnesium hydride, similar temperatures of the order of 573 K are required for desorption at around one bar of hydrogen pressure. The main drawback of using $LiBH_4$ is the difficulty to rehydrogenate. Usually, elevated temperatures of around 873 K and pressures of the order of 150 bar are needed for $LiBH_4$ formation from the decomposition products [3–5].

$$LiH + B + 3/2H_2 \leftrightarrow LiBH_4 \quad (1)$$

Recently, an interesting way to destabilize $LiBH_4$ has been proposed by Vajo *et al.* [6] as well as Barkhordarian *et al.* [7]. In this scheme, by adding a second element or hydride, a secondary exothermal reaction is taking place during dehydrogenation, thus effectively reducing the overall heat of reaction. Recent studies have explored this way of destabilization [8–10].

However, in order to fully take advantage of this approach, a better fundamental knowledge of the constituents is needed. The $LiBH_4$ crystal structure, phase transition, and phonons modes have been investigated, mainly by X-ray diffraction [11–18], Raman spectroscopy [15,19–23], NMR [18,24,25], and calorimetry [18,26].

At low temperature, $LiBH_4$ crystallizes with an orthorhombic structure (space group P*nma*), where each $(BH_4)^-$ anion is surrounded by four Li^+ cations in a tetrahedral configuration and each Li^+ is surrounded by four $(BH_4)^-$ anions also in a tetrahedral configuration [11]. The high temperature crystal structure is hexagonal (space group P6_3mc) and closely related to the orthorhombic room temperature phase. In the high temperature phase, the tetrahedrons are more symmetric and less distorted than in the orthorhombic phase [11]. The orthorhombic (low temperature) → hexagonal (high temperature) first order phase transition appears at around 383 K [1,4,20,27]. It has been observed that a slight hydrogen desorption of 0.3 to 1.3 wt.% takes place in the region of the structural phase transformation [1,18,28]. At ambienttemperature, a phase transition into a high-pressure phase (A*ma2*) is observed around0.6 GPa, and a second transition at ca 18 GPa leads to a cubic phase (F*m-3m*) [13].

In many experimental set-ups $LiBH_4$ or a mixture of it with other compounds is milled in order to achieve nanocrystallinity and better hydrogen sorption properties. However, it is well known that milling also introduces phase transformation. In this paper, we report a calorimetric investigation of phase transformation in unmilled and ball-milled $LiBH_4$. We also tested the effect of air exposure on the phase transitions behaviour of unmilled $LiBH_4$.

2. Experimental Method

The $LiBH_4$ used in this investigation was purchased from Sigma-Aldrich and had a purity of 95%. High energy milling was carried out in a Spex 8000 shaker mill. Each milling was performed by placing one gram of $LiBH_4$ inside a 55 cm^3 hardened steel crucible in an argon atmosphere with three stainless steel balls for a ball to powder weight ratio of 30. After 1 h of milling a fine powder was collected and stored under argon.

The Pressure Differential Scanning Calorimetry (PDSC) was performed on a Q10 apparatus from TA Instrument Company. Sample pans and covers made of copper were used. The pans were loaded with $LiBH_4$ and the cover crimped in an argon filled glove box. The crimped samples pans were put in a small vial under argon and were exposed to the air just for loading the sample on the PDSC instrument. As the samples were crimped, the air exposure is essentially nil. PDSC runs were performed under argon atmosphere, as well as under 2 bar of hydrogen. As hydrogen diffusion is high, the fact of using crimped samples does not prevent release and uptake of hydrogen by the sample. In most cases, three successive runs were performed in each experiment. A first heating run from room temperature to 425 K, was followed by a cooling run from 425 K to room temperature and a last heating run up to 425 K. The heating and cooling rates were the same (in absolute value) for the three successive runs. Heating (cooling) rates of 40, 20, 10, 5, and 2 K/min were used. For the cooling curves, the lowest temperature reached is much higher for runs done under argon than for the ones done under hydrogen. This is explained by the fact that the PDSC apparatus does not have a cooling unit; therefore the cold source of the apparatus is actually the room. As argon has much lower heat conductivity than hydrogen, the heat exchange between the PDSC block and the room is much better when hydrogen gas is used instead of argon. In the cooling mode, the program tries to maintain the requested temperature ramp but, when cooling power is not sufficient and the set ramp cannot be maintained, the execution of the program stops. Heat conductivity of argon being smaller than hydrogen, this is why the cooling runs stop at a higher temperature for runs performed under argon compared to hydrogen.

For air exposure experiments we used dry air from Praxair of *Volatile Organic Compound Free* grade with less than 2 ppm of water. The applied pressure was 120 bar. X-ray powder diffractions (XRD) were performed on a Bruker D8 Focus diffractometer using Cu Kα radiation.

In-situ powder diffraction under Ar and H_2 atmosphere were performed at the Swiss-Norwegian Beam Lines of ESRF. Diffraction data for the ball-milled $LiBH_4$were collected on a 0.5 mm glass capillaries filled in a high purity Ar-atmosphere. A MAR345 Imaging Plate detector at the sample-to-detector distance of 250 mm and synchrotron radiation at λ = 0.700090 Å were used. The capillary was heated from 100 K to 500 K at a rate of 10 to 100 K per hour, while synchrotron powder diffraction data were collected *in-situ*. Temperature was controlled with an Oxford Cryostream 700+. Each pattern was collected during 50–60 seconds exposure time, while the capillary was rotated by 50–60 degrees, followed by a readout during 83 seconds.

The following *in-situ* diffraction experiments were performed under Ar atmosphere:

- Wide temperature range: upon heating from 100 to 500 K, with 60 K per hour rate;

- Fine temperature sampling: upon heating from 368 to 398 K, followed by cooling in the same temperature range with a rate of 10 K per hour; the same heating/cooling cycle was then repeated on the same sample spot, but with a rate of 100 K per hour.

Under hydrogen pressure, the following *in-situ* diffraction experiments were performed, using the gas system described in [29]:

- Under 2 bar of H_2: first upon heating from 297 to 400 K with a rate of 40 K per hour and then on cooling from 400K to 350 K with a rate of 100 K per hour;
- Under 40 bar of H_2: upon heating from 350 to 395 K, with a rate of 20 K per hour.

The data were integrated using Fit2D program [30] and a calibration measurement of a NIST LaB_6 standard sample. Very high counting statistics allowed us to define precisely the background line and to observe very weak diffraction peaks. Highly accurate integrated intensities were obtained thanks to a good powder average achieved by projecting the 3D scattering information on the 2D detector.Uncertainties of the integrated intensities were calculated at each 2θ-point by applying Poisson statistics to the intensity data, considering the geometry of the detector, similar to the procedure described in [31]. The calculated absorption coefficient is practically equal to zero, thus the absorption correction was not applied.

Structural information for the orthorhombic and the hexagonal phases of $LiBH_4$ was taken from [14]. Temperature dependence of the cell and other structural parameters was obtained via a sequential Rietveld refinement implemented into Fullprof [32]. Positions and thermal displacements of Li and BH_4 groups were refined according to [14]. The background was described by linear interpolation between selected points.

3. Results and Discussion

3.1. Structural Characterization

Figure 1 shows the X-ray powder diffraction of unmilled and milled $LiBH_4$. As a comparison a calculated pattern of the low temperature orthorhombic phase as given in Refs. [11,12,14] is also shown. It should be pointed out that, because $LiBH_4$ reacts with water vapour contained in air, a sealed sample holder had to be used for X-ray powder diffraction measurements. This sample holder is responsible for the large background between 10 and 40 degrees. In the case of unmilled (as-received) sample only two peaks could not be indexed to the $LiBH_4$orthorhombicphase: one peak at around 16° and the other peak at around 22°. These two peaks could not be indexed to any oxide or hydroxide phase and their origin is still unknown. The most striking feature of the diffraction pattern of unmilled sample is an altering of the relative intensity of the diffraction peaks. In Figure 1, the Miller indices of the peaks with intensities much higher than the calculated pattern are given.

Figure 1. X-ray powder diffraction of unmilled and one hour milled $LiBH_4$.

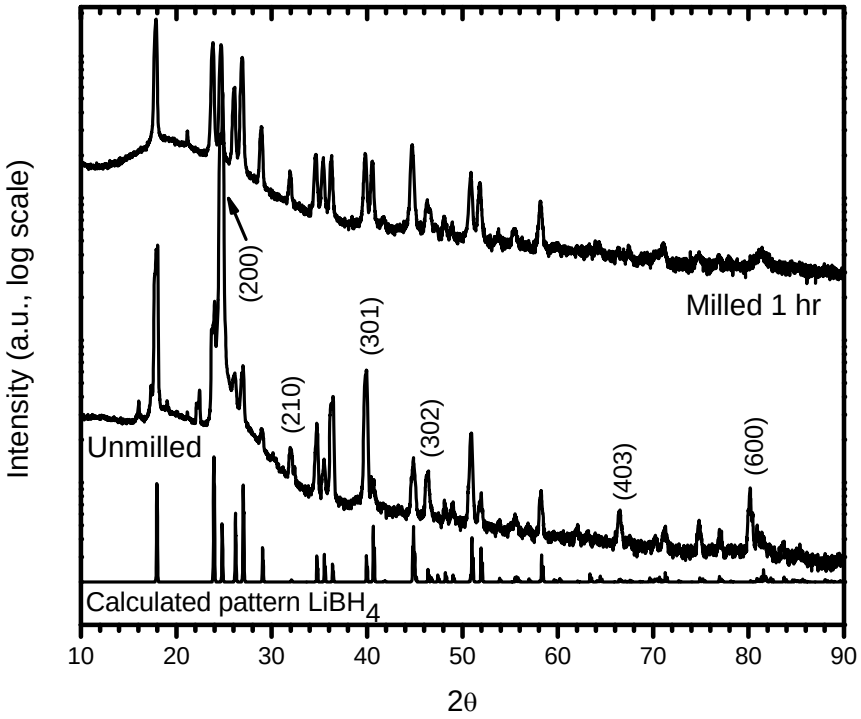

In the case of ball milled sample, the bad powder average [14] and preferred orientation seen in the unmilled pattern have been eliminated and the relative intensities are very close to the calculated pattern. The most probable explanation for the features of unmilled and milled samples is that the synthesis method induced some texture to $LiBH_4$ particles and when the particles are broken by ball milling action this texture is lost. Surprisingly, the two unknown peaks present in the unmilled sample pattern are no longer visible in the milled sample curve. In fact the only peak that does not belong to $LiBH_4$ phase in the pattern of milled sample is a very small peak at around 21°.

3.2. Phases Transformations in Unmilled $LiBH_4$

Figure 2 shows the DSC curves of unmilled $LiBH_4$ taken under argon atmosphere, 2 bar of hydrogen with a 20 K/min ramp. The peak temperatures of the different events are listed in Table 1. Each curve shows a first heating (H1) from room temperature to 415 K followed by a cooling curve (C) from 415 K to the lowest temperature reachable while keeping the 20 K/min cooling rate, and a second heating (H2) to 415 K. Figure 2 shows several interesting features. First, a small endotherm around 318 K is present on the curve recorded under argon atmosphere but is absent on the curve recorded under 2 bar of hydrogen. This endotherm was reported before but its nature was not discussed [18]. The character of this endotherm will be examined further in the following sections. Secondly, a large exotherm is seen between the first endotherm and the usual low temperature → high temperature phase transition endotherm *i.e.*, from about 330 K to 385 K. This exotherm was reported by Mosegaard *et al.* for an air exposed sample and was coupled with hydrogen release [18]. They attributed it to a complex between water and $LiBH_4$ and associated it to an additional phase. On the other hand, Kato *et al.* reported hydrogen release centered at the phase transition temperature for pure $LiBH_4$ as well as for

$LiBH_4$ exposed to oxygen [33]. As will be seen in the next sections, our tests indicate that gas release at around the phase transition temperature is not a matter of contamination but an intrinsic characteristic of the material.

Figure 2. Scanning PDSC traces under argon (A) and 2 bar hydrogen pressure (B) of unmilled $LiBH_4$. H1: first heating run; C: first cooling; H2: second heating run. Heating and cooling rates: 20 K min^{-1}.

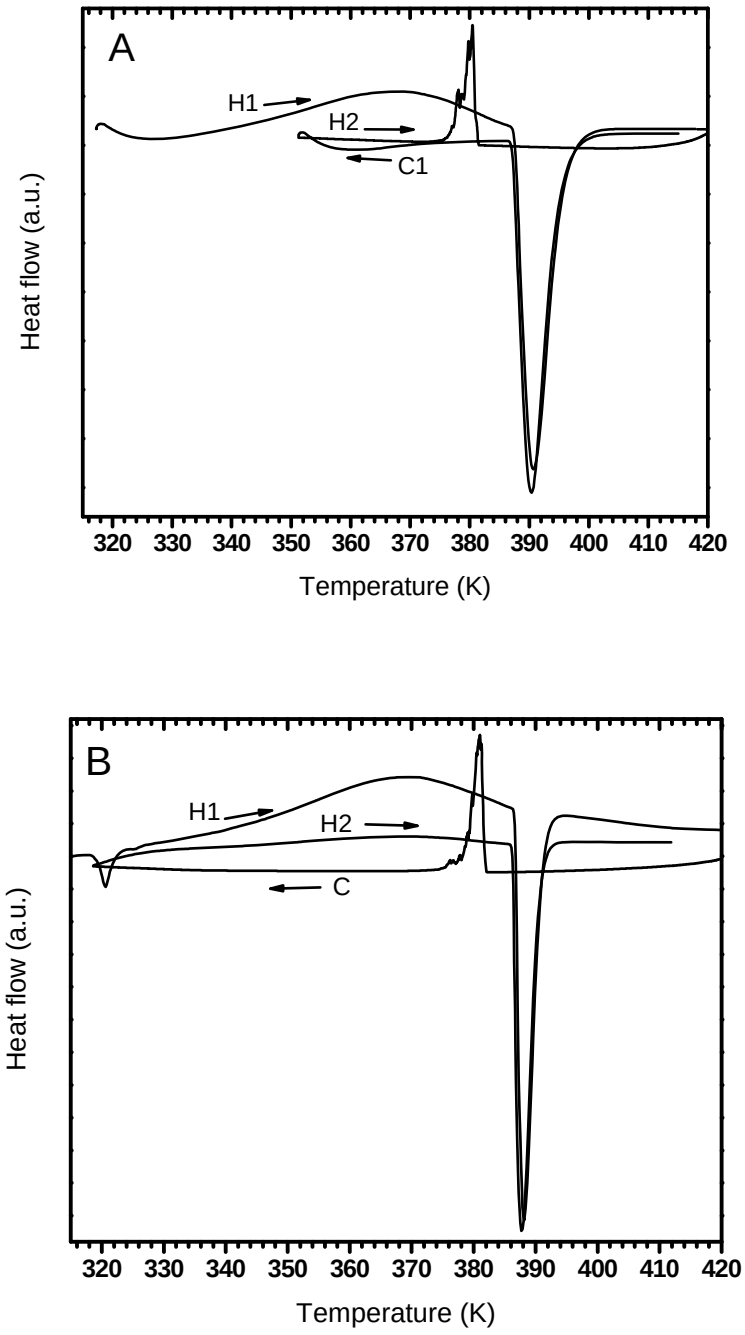

Table 1. Peak temperature (in K) measured in PDSC scans of unmilled $LiBH_4$. Heating and cooling rates: 20 K min^{-1}. Uncertainty in all measurements is ± 0.1 K.

	First heating			First cooling	Second heating	
DSC atmosphere	First endotherm	Exotherm	Phase transition	Phase transition	Exotherm	Phase transition
Argon	--	368.3	390.6	380.4	--	390.3
2 bar Hydrogen	320.6	367.7	388.1	381.0	368.9	387.6

The low temperature → high temperature phase transition endotherm measured in our investigation is in the same temperature range than reported in previous investigations [1,4,20,27]. A close inspection of the phase transition endotherms shows that the curves measured under argon atmosphere are not as steep as the ones measured under hydrogen. This is most probably due to the higher conductivity of hydrogen which produces a faster kinetic of the phase transformation and thus a steeper slope.

Upon cooling, the high temperature → low temperature phase transition is seen at a temperature of about 381 K. This hysteresis was identified by Gomes at al. and was explained by the fact that the transition is of first order [20]. In Table 1 the peak temperature of all events are presented. We see that the nature of PDSC atmosphere does not have a major impact on peak temperatures.

3.3. Investigation of the Exotherm

3.3.1. Effect of PDSC Atmosphere

From Figure 2, the qualitative behaviour of the exotherm curve can be determined. First, the exotherm appears on the heating part of the curves but is practically absent in the cooling curves no matter if the experiment was performed under argon or hydrogen atmospheres. As the exotherm appears in the first heating for both argon and hydrogen atmosphere we can rule out immediately that the exotherm is due to the different heat conductivity of these two gases. Secondly, on the second heating (H2) the exotherm is present for experiments run under hydrogen but is absent for the experiments run under argon. To have a better proof of these observations, the following experiment was performed. First, an unmilled $LiBH_4$ sample was subjected to three successive PDSC heating under a hydrogen pressure of 2 bar. After each run the sample was cooled in the DSC under the same atmosphere. As seen on Figure 3A, the successive runs are almost identical. The orthorhombic-hexagonal phase transformation happens at the same temperature and the exotherm is present in all curves. The only noticeable difference is the disappearance of the low temperature endotherm for the second run. However, this endotherm re-appears on the third run. The reason for this effect is unclear. As the exact nature of this endotherm has not been discussed in the literature, this question remains open.

Figure 3. Successive scanning PDSC traces of unmilled $LiBH_4$. (A): All runs performed under 2 bar of hydrogen pressure. (B): First run and third run under 2 bar of hydrogen, second run under argon. Heating and cooling rates: 20 K min^{-1}.

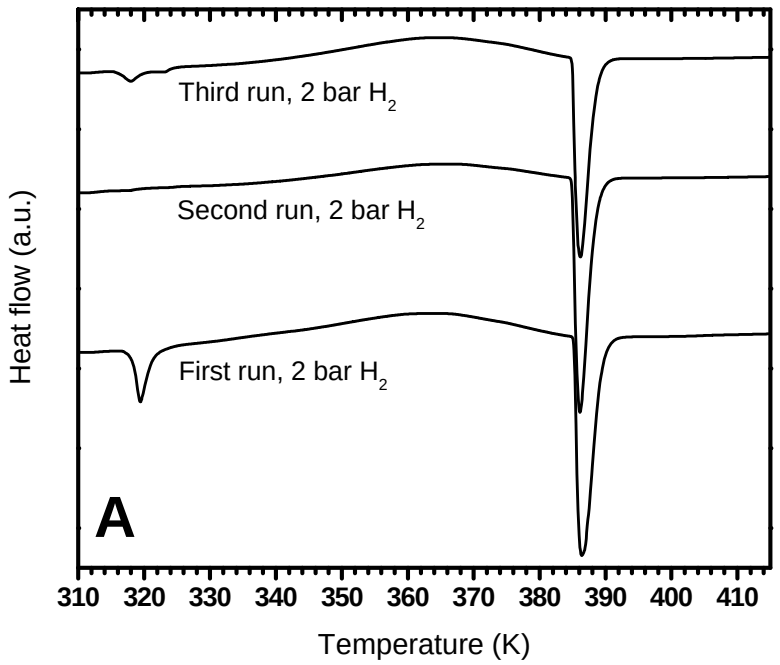

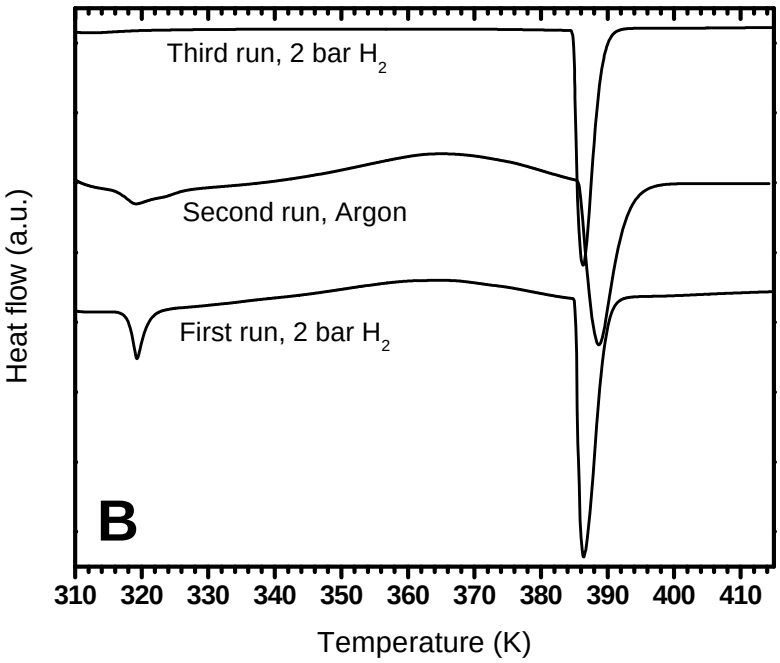

For the second test, a new unmilled $LiBH_4$ sample was subjected first to a heating and cooling under 2 bar of hydrogen. The PDSC atmosphere was then changed to one bar of argon and a second heating/cooling cycle performed. After completion of the second cycle, the PDSC atmosphere was returned to 2 bar of hydrogen and a third cycle was carried out. The DSC traces of these runs are shown in Figure 3B. As expected, the first run is identical to the one seen in Figure 3A. In the same

way, the second run is showing the same features as in Figure 2, *i.e.*, endotherm at 318 K, broad exotherm and different slope of the low orthorhombic-hexagonal phase transformation due to the different atmosphere. However, a drastic difference is seen for the third run. This curve does not show the low temperature endotherm as well as the broad exotherm. Only the orthorhombic-hexagonal phase transformation is seen. Therefore, after a complete cycle under argon the nature of the sample changed, contrary to the case for the experiment performed entirely under hydrogen. In a separate experiment (not shown), we confirmed that if the third run is also performed under argon the curve is identical to the second run under argon reported in Figure 3B.

3.3.2. Effect of Settling Time

The preceding section results seem to indicate that argon atmosphere "degrades" $LiBH_4$in some way. We also suspected that time might play a role in this change of thermodynamic behaviour. We thus executed the following experiment: a heat/cool/heat run under argon was carried out on an unmilled $LiBH_4$ sample. The sample was then stored in an argon atmosphere glove box for two days. After this period the sample was measured again under the same conditions. The resulting PDSC curves are presented in Figure 4. The first experiment is identical to the one reported in Figure 2 and it is clear that on the second run the exotherm is not present. The remarkable result is that after two days in the glove box the sample has a PDSC trace identical to the original one. Mainly, the broad exotherm is totally recovered. Therefore, we may conclude that after a PDSC run under argon $LiBH_4$ is in a metastable state. The reason why such a metastable state is reached while the scan is performed under argon and not when it is under hydrogen has to be investigated. One possible explanation may be related to the slight desorption of hydrogen at temperature below the orthorhombic-hexagonal phase transformation seen by Soulié *et al.* [11]. Our hypothesis is that maybe some hydrogen is in solid solution in the $LiBH_4$ structure. When the compound is heated and cooled under hydrogen atmosphere, some hydrogen will return in solid solution during the cooling phase. However, if the heating/cooling is done under argon, the amount of hydrogen liberated during heating is so small that it will get diluted into the argon atmosphere and the partial pressure will be too low to re-enter $LiBH_4$ during the cooling phase. If then a second run is performed immediately after the first run, there will be no release of hydrogen during heating. However, if the sample is left for some time, an equilibrium solid solution is forming again by a slight dehydrogenation of $LiBH_4$. As this quantity of hydrogen is very small compared to the total hydrogen capacity of $LiBH_4$, this phenomena is virtually impossible to see by powder diffraction. Thermodynamically, a release of hydrogen is usually an endothermic effect, thus the low temperature endotherm may be the release of hydrogen in solid solution. Once this hydrogen is released, the crystal structure should accommodate to a new environment, thus producing the large exotherm.

Figure 4. Scanning PDSC traces under argon of unmilled $LiBH_4$ before and after two days of storage in a glove box. Heating and cooling rates: 20 K min^{-1}.

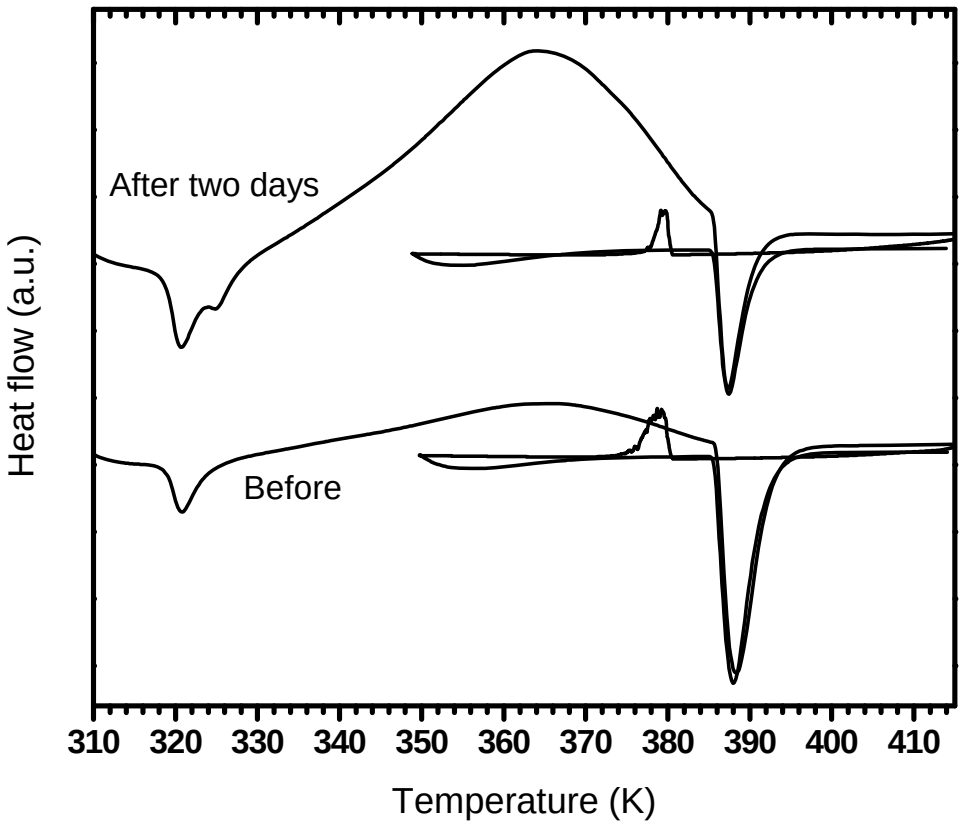

3.3.3. Effect of Exposure to Dry Air

Previous reports have attributed the presence of the exotherm either as a complex between water and $LiBH_4$ [18] or as decomposition of etherates [34]. In a recent report, Kato *et al.* have shown that exposure to oxygen significantly enhances the hydrogen desorption process and reduces desorption of diborane [33]. They also showed that oxygen exposure induces segregation of Li onto the surface. In the present investigation we measured the effect of air expose upon the thermal behaviour of $LiBH_4$. For this purpose, a sample of unmilled $LiBH_4$ was put inside a pressured vial which was filled with dry air at 20 bar and kept at room temperature for two days. After two days of dry air exposure, a PDSC curve under argon was performed. Figure 5 shows the results of the PDSC heating/cooling/heating scan after two days of dry air exposure. In Table 2 we list the peak temperatures for scans before and after air exposure. It is clear that there are no obvious changes on the presence and peak temperature of the various exothermic and endothermic reactions. Therefore, we could conclude that dry air exposure does not have any effects on the thermodynamics of phase transition in $LiBH_4$.

Table 2. Peak temperature (in K) measured in PDSC scans of unmilled $LiBH_4$ before and after air exposure. Heating and cooling rates: 20 K min^{-1}. Uncertainty in all measurements is ± 0.1 K.

	First heating			First cooling	Second heating	
Sample	First endotherm	Exotherm	Phase transition	Phase transition	Exotherm	Phase transition
Before air exposure	319.6	362.6	385.9	378.8	364.4	386.1
After two days air exposure	320.8	365.0	389.4	378.6	--	389.1

Figure 5. Scanning PDSC trace under argon of unmilled $LiBH_4$ after two days of air exposure. Heating and cooling rates: 20 K min^{-1}.

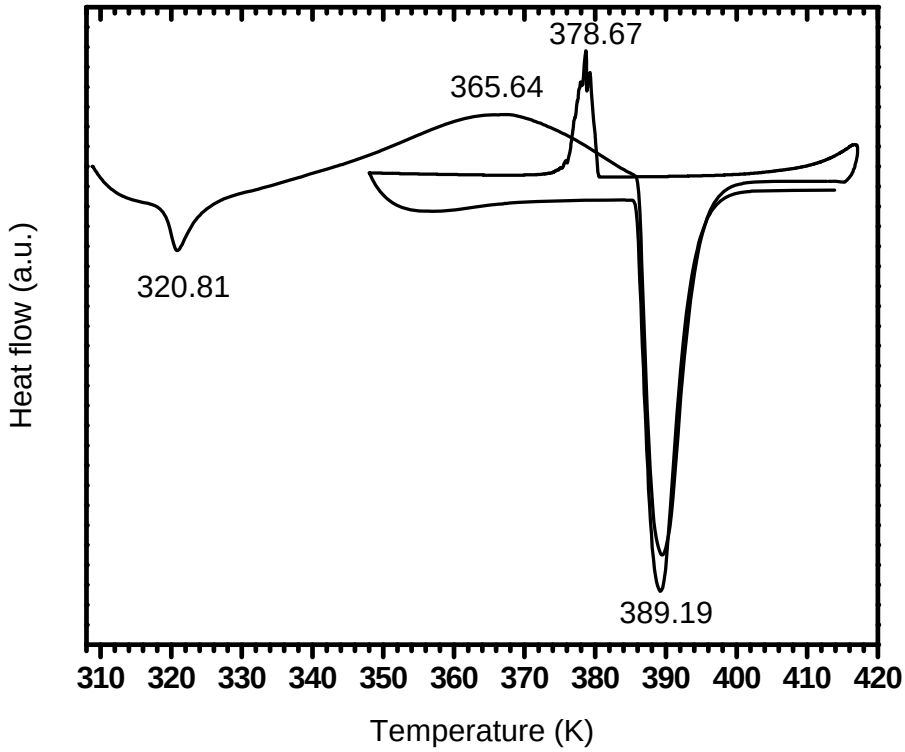

3.4. Effect of Milling

In this section we will report on the effect of high energy ball milling of $LiBH_4$. Samples of as-purchased $LiBH_4$ were milled for one hour in a high energy mill under argon atmosphere.

3.4.1. PDSC Curves

The PDSC curves under different atmosphere of ball milled $LiBH_4$ are shown in Figure 6. These curves are drastically different than the unmilled $LiBH_4$ curves of Figure 2. In the following sections, we will examine in details the features of PDSC curves taken under various atmospheres on the milled sample.

Figure 6. Scanning PDSC traces under argon and hydrogen pressure of one hour milled $LiBH_4$. Heating and cooling rates: 20 K min^{-1}

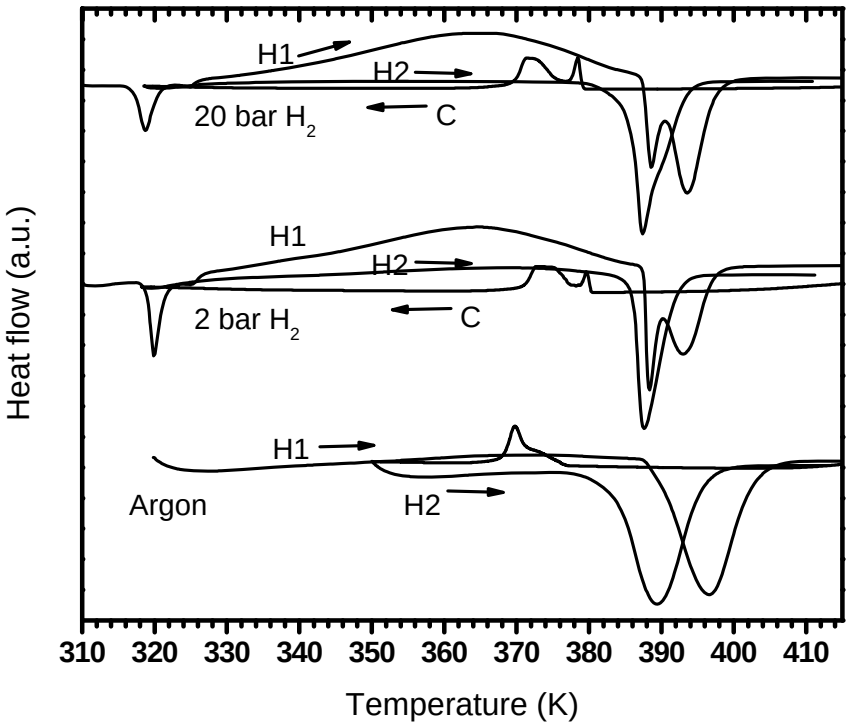

3.4.1.1. PDSC Performed under Argon Atmosphere

For the PDSC run done under argon atmosphere we see that on the first heating (H1) the low temperature → high temperature phase transition presents an endotherm that is much broader and at a higher temperature than in the unmilled $LiBH_4$ case. The cooling curve shows an exotherm peak corresponding to the high temperature → low temperature phase transition that is broader and at lower temperature than the corresponding transition for the unmilled case of Figure 2. On the second heating curve (H2), the endotherm peak temperature is shifted back to the same temperature as in the unmilled case except that the peak is still very broad.

3.4.1.2. PDSC Performed under Hydrogen Atmosphere (2 and 20 bar)

For the milled material, the most significant feature of the PDSC runs under hydrogen is the appearance of a double peak at the temperature of the low temperature → high temperature phase transition. In the case of the first heating (H1), these double peaks are formed by a small sharp peak at the same temperature as the phase transition peak seen in the unmilled case followed by a broad peak at higher temperature. In the cooling run (C), there is also a double peak with the sharp peak corresponding to the one present in the unmilled sample and a broad peak at lower temperature. On second heating (H2), the sharp peak is more important and the broad peak shifted to lower temperature and could be seen only as a shoulder of the sharp peak. These features are essentially the same for runs performed under 2 bar and 20 bar of hydrogen. The broad peak may be due to re-crystallization of the small $LiBH_4$ particles.

3.4.2. Activation Energy of the Exothermic Peak

In order to get more information on the nature of the exothermic peak, PDSC scans were performed at heating rates 2, 5, 10, 20, and 40 K/min under argon atmosphere and 2 bar of hydrogen pressure for unmilled and milled samples. Figure 7 shows the curves under 2 bar of hydrogen for milled $LiBH_4$. Even if the scale had to be changed in order to fit all curves, it can be seen that the exotherm peak shifts to lower temperatures when the heating rate is reduced. The activation energy, as determined from Kissinger's plots, is reported in Table 3. It shows that, except for the unmilled sample measured under argon, all other values are in agreement within experimental errors. Therefore, milling does not seem to change the nature of the exothermic peak.

Table 3. Activation energies in kJ/mol of the exothermic peak of unmilled and one hour milled $LiBH_4$.

Atmosphere / Sample	argon	2 bar hydrogen
Unmilled	79 ± 6	102 ± 2
Milled	95 ± 8	100 ± 12

Figure 7. Scanning PDSC traces under 2 bar of hydrogen pressure of one hour milled $LiBH_4$.

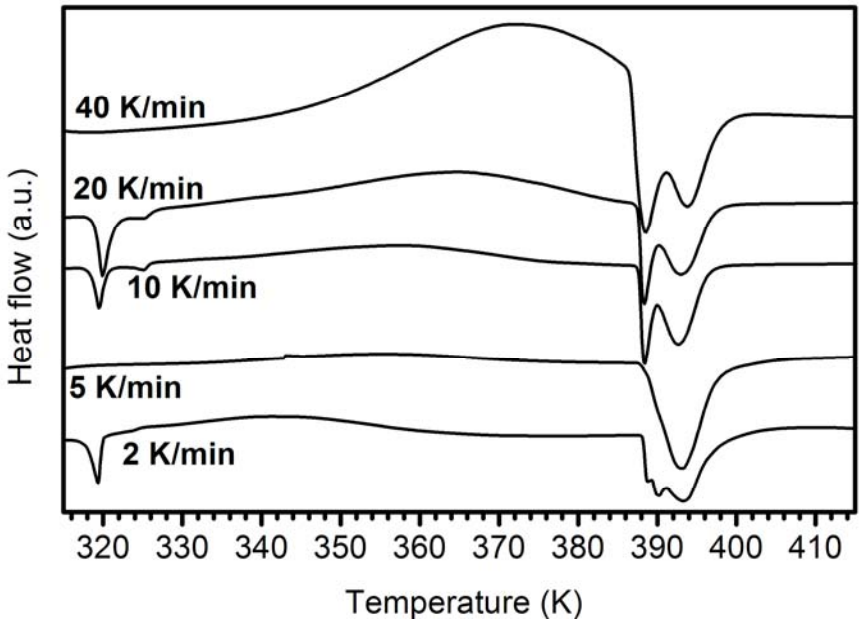

3.5. In-situ Synchrotron X-ray Diffraction Study

As mentioned in the experimental section, synchrotron *in-situ* powder diffraction was performed for ball milled $LiBH_4$. Representative Rietveld refinements of patterns taken below (100 K) and above (388 K) the phase transition are presented in Figure 8. Both refinements show single phase samples without any impurities. A search for an intermediate phase was done by heating and cooling under argon and hydrogen pressures (2 bar and 40 bar) as described in the experimental section. As a representative of these measurements Figure 9 shows the stack of powder diffraction patterns for a sample heated from 297 K to 400 K at 40 K per hour and under 2 bar of hydrogen pressure. It is clear

that there are no unidentified peaks and the transition goes directly from the orthorhombic to the hexagonal phase. A similar situation was observed for all other cases of heating and cooling, irrespective of the nature of gas (argon or hydrogen), pressure and rate of heating. No evidence of a new phase was found. However, some interesting observations were made on the temperature variation of the unit cell parameters.

Figure 8. Rietveld refinement profile for the ball-milled $LiBH_4$ sample measured at 100 K (Top) and 388 K (Bottom), $\lambda = 0.700090$ Å.

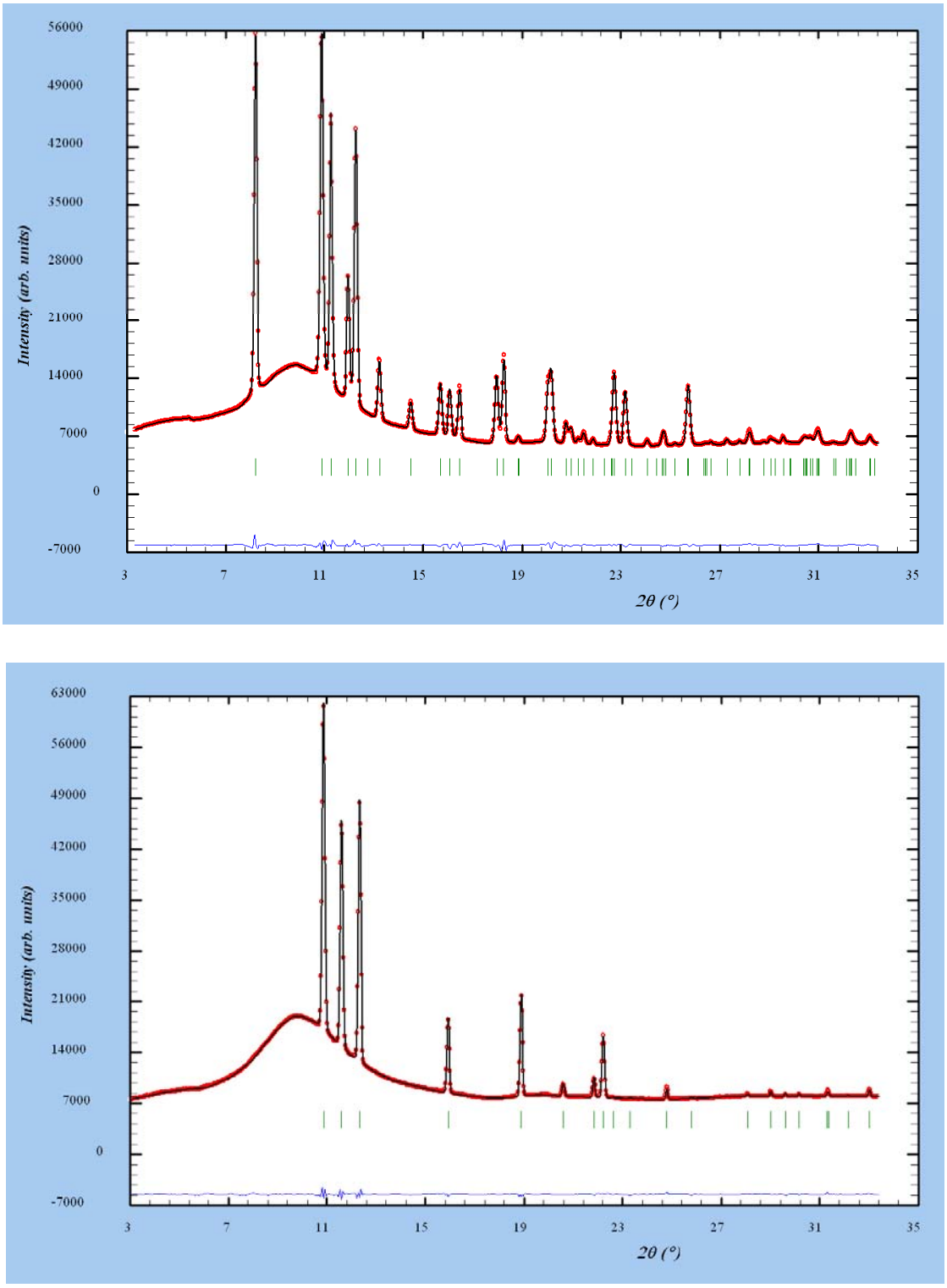

Figure 9. *In-situ* SR-XRD patterns of ball milled $LiBH_4$ during heating from 297 K to 400 K under 2 bar of hydrogen. Heating rate: 40 K/min. λ = 0.700090 Å.

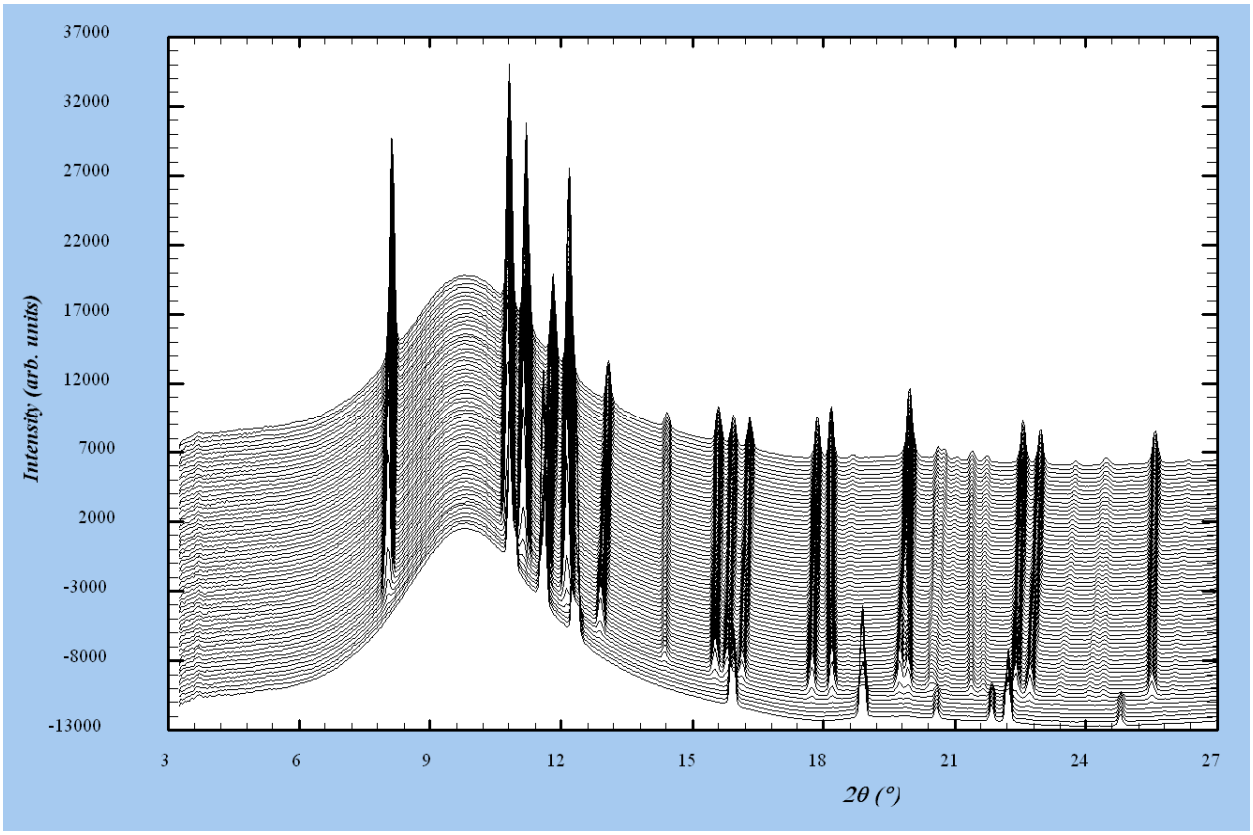

3.5.1. Temperature Variation of Lattice Parameters: Effect of Milling

Cell parameters for the orthorhombic $LiBH_4$ phase, measured under Ar upon heating from 100 to 500 K with 60 K per hour rate, are plotted in Figure 10 with those for the unmilled sample reported in ref. [14]. A large discrepancy is observed at low temperatures. This difference is probably related to the strains induced by milling. The data from image plate detector have a good time resolution which is perfectly suited for the *in-situ* measurements of this investigation. On the other hand, they are not of sufficiently high angular resolution for the accurate determination of strain parameters. Hydrogen desorption may release some strain in the milled $LiBH_4$, but an observation of the strain decrease would be difficult to interpret as this might be the result of any other relaxation process.

At higher temperatures (above 300 K), the variation of the cell parameters corresponds to an evolution of the order parameter driving the temperature-induced phase of the orthorhombic $LiBH_4$. It has been shown that the order parameter in $LiBH_4$ can be parameterized as a shift of layers formed by Li and BH_4, together with in-layer deformations [35]. The temperature dependence of Li-B distances has shown [15] that the layers defined in the *bc* plane of the orthorhombic phase become flatter as the temperature is increased: the difference between atomic coordinates for Li and B atoms decreases with temperature. Also, the distance between the layers significantly increases with temperature.

Figure 10. Lattice parameters **a** (top), **b** (middle), and **c** (bottom) of orthorhombic $LiBH_4$ as a function of temperature during heating under argon atmosphere. Unmilled $LiBH_4$: black symbols ([14]), milled $LiBH_4$: red symbols.

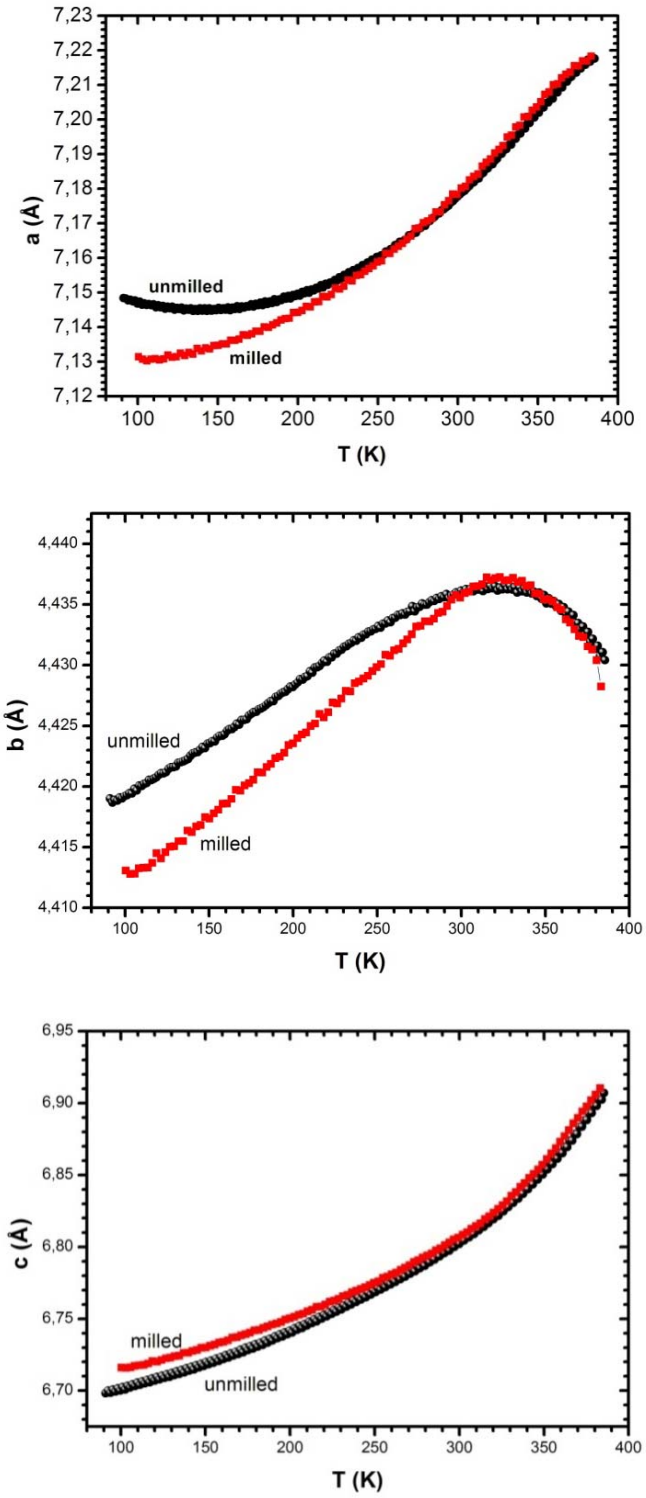

However, the pronounced difference between the milled and unmilled samples occurs only at low temperatures, where a bistability of the low-temperature *Pnma* and high-pressure *Ama*2 phases of $LiBH_4$ is observed [23]. Thus, the strains make an influence not on the temperature driven phase

transition (*Pmna* ↔ $P6_3mc$) but on the pressure driven one (*Pnma* ↔ *Ama*2). The hypothesis is that milling should move the boundary of the *Pnma*↔*Ama*2 phase transition.

3.5.2. Temperature Variation of Lattice Parameters: Effect of Hydrogen Atmosphere and of a Hydrostatic Pressure

The axial ratios are sensitive to different external stimuli, and they are quite accurate, since they do not depend on the absolute values of the cell parameters (*i.e.*, instrument calibration etc). The axial ratios measured under argon and hydrogen for milled and unmilled samples are reported in Figure 11. These plots unambiguously prove the pronounced effect of milling on the thermal expansion of $LiBH_4$.Curves of milled samples measured under argon (black circles) and under 2 bar of hydrogen (blue lozenges) are identical. However, the milled sample measured under 40 bar of hydrogen is clearly different from the others. Unfortunately the sample under 40 bar H_2 was not measured down to low T, but even with the data in the limited T-range, the effect of H_2 pressure is undeniable.

Analysis of the high-pressure data collected on the LT $LiBH_4$ in diamond anvil cells [13] yields the following previously unpublished pressure dependences of its cell parameters:

$$a = 7.1772(6)–0.2670(9)\ P \quad (1)$$

$$b = 4.4461(3)–0.0635(5)\ P \quad (2)$$

$$c = 6.8251(6)–0.074(1)\ P, \quad (3)$$

where P is in GPa and the number in parentheses is the uncertainty on the last digit.

Despite the fact that the compression of the *a*-parameter is more pronounced, the observed temperature variations of the axial ratios (Figure 11) cannot be explained merely as an effect of pressure. The observed change between 0 and 40 bar of H_2indicates an interaction between the hydrogen gas and the LT $LiBH_4$ solid phase.

Figure 11. Axial ratios of the orthorhombic $LiBH_4$ measured under argon in its milled (red squares, 100–383 K) and unmilled (black circles, 91–385 K [14]) states compared with those for milled $LiBH_4$ measured under 2 (blue lozenges, 297–386 K) and 40 (green triangles, 350–385 K) bar of hydrogen.

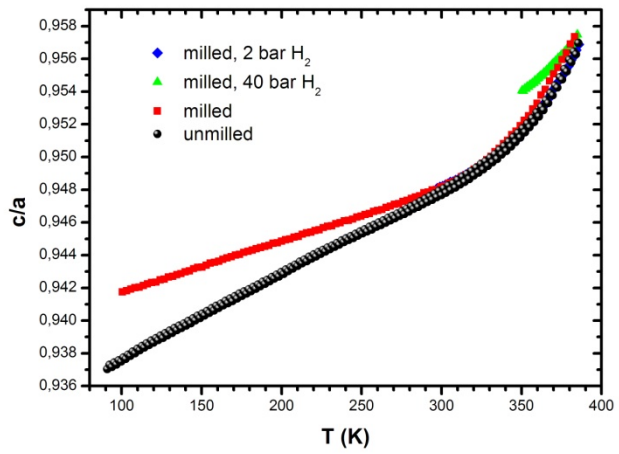

Figure 11. *Cont.*

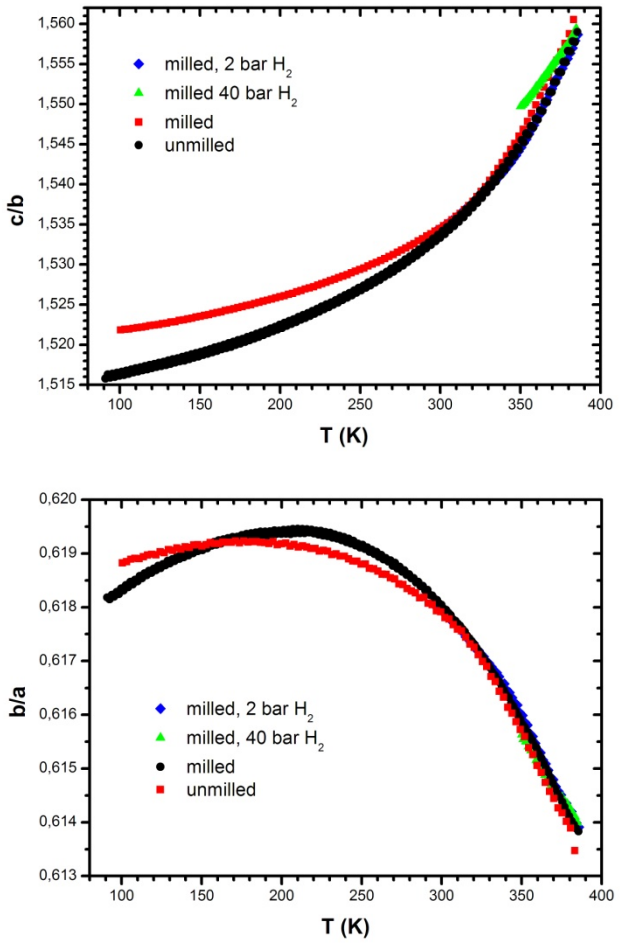

In principle, the amount of hydrogen absorbed could be determined from the observed volume deviations. Unfortunately the values of the cell volume are accurate only within the range of the same experiment. So, any relative volume changes can be monitored by cycling the sample in vacuum or in hydrogen atmosphere which could not be done with our experimental conditions. Therefore, the estimation of the hydrogen trapped in solid solution in the LT $LiBH_4$ solid phase is not possible.

4. Conclusion

We studied the effect of milling and air exposure on the thermodynamic and crystal structure properties of $LiBH_4$. The presence of an exothermic peak before the low temperature → high temperature (orthorhombic → hexagonal) phase transition was shown not to be due to air contamination. From PDSC measurements under argon and hydrogen atmospheres, it was revealed that this exotherm is closely related to the presence of hydrogen and has an activation energy of 100 kJ mol^{-1} (1 eV). It is thus postulated that it is due to some hydrogen evolution in solid solution in the orthorhombic low temperature $LiBH_4$ phase. It was also found that, upon milling, the endothermic peak of the orthorhombic → hexagonal phase transition is split in two when the PDSC scan is performed under hydrogen. However, no sign of another crystal structure was found from *in-situ* synchrotron diffraction studies. On the other hand, synchrotron measurements showed that lattice

parameters are altered by milling due to induced strain. These strains do not change the boundary of the temperature-driven phase transition (*Pmna* ↔ *P*6$_3$*mc*) but may modify the pressure driven transition (*Pnma* ↔ *Ama*2). The axial ratios for the LT $LiBH_4$ are considerably different under 40 bar of hydrogen, indicating an interaction between the hydrogen gas and the LT $LiBH_4$ solid phase.

Acknowledgements

The authors would like to thank F. Morin for help in X-ray powder diffraction, D. Chernyshov for helpful discussions, J. Goyette of UQTR for reviewing the manuscript and SNBL for in-house beamtime allocation. This project was supported by Natural Resources Canada and National Science and Engineering Council.

References

1. Züttel, A.; Rentsch, S.; Wenger, P.; Sudan, P.; Mauron, P.; Emmenegger, C. Hydrogen storage properties of $LiBH_4$. *J. Alloys Compounds* **2003**, *356–357*, 515–520.
2. Friedrichs, O.; Kim, J.W.; Remhof, A.; Buchter, F.; Borgschulte, A.; Wallacher, D.; Cho, Y.W.; Fichtner, M.; Oh, K.H.; Züttel, A. The effect of Al on the hydrogen sorption mechanism of $LiBH_4$. *Phys. Chem. Chem. Phys.* **2009**, *11*, 1515–1520.
3. Mauron, P.; Buchter, F.; Friedrichs, O.; Remhof, A.; Bielmann, M.; Zwicky, C.N.; Zuttel, A. Stability and Reversibility of $LiBH_4$. *J. Phys. Chem. B* **2008**, *112*, 906–910.
4. Orimo, S.; Nakamori, Y.; Kitahara, G.; Miwa, K.; Ohba, N.; Towata, S.; Züttel, A. Dehydriding and rehydriding reactions of $LiBH_4$. *J. Alloys Compounds* **2005**, *404–406*, 427–430.
5. Friedrichs, O.; Buchter, F.; Borgschulte, A.; Remhof, A.; Zwicky, C.N.; Mauron, P.; Bielmann, M.; Züttel, A. Direct synthesis of $Li[BH_4]$ and $Li[BD_4]$ from the elements. *Acta Mater.* **2008**, *56*, 949–954.
6. Vajo, J.J.; Skeith, S.L.; Mertens, F. Reversible Storage of Hydrogen in Destabilized $LiBH_4$. *J. Phys. Chem. B* **2005**, *109*, 3719–3722.
7. Barkhordarian, G.; Klassen, T.; Dornheim, M.; Bormann, R. Unexpected kinetic effect of MgB_2 in reactive hydride composites containing complex borohydrides. *J. Alloys Compounds* **2007**, *440*, L18–L21.
8. Yang, J.; Sudik, A.; Wolverton, C. Destabilizing $LiBH_4$ with a Metal (M = Mg, Al, Ti, V, Cr, or Sc) or Metal Hydride (MH_2 = MgH_2, TiH_2, or CaH_2). *J. Phys. Chem. C* **2007**, *111*, 19134–19140.
9. Alapati, S.V.; Johnson, J.K.; Sholl, D.S. Large-Scale Screening of Metal Hydride Mixtures for High-Capacity Hydrogen Storage from First-Principles Calculations. *J. Phys. Chem. C* **2008**, *112*, 5258–5262.
10. Bösenberg, U.; Doppiu, S.; Mosegaard, L.; Barkhordarian, G.; Eigen, N.; Borgschulte, A.; Jensen, T.R.; Cerenius, Y.; Gutfleisch, O.; Klassen, T., *et al.* Hydrogen sorption properties of MgH_2-$LiBH_4$ composites. *Acta Mater.***2007**, *55*, 3951–3958.
11. Soulié, J.-P.; Renaudin, G.; Cerny, R.; Yvon, K. Lithium boro-hydride $LiBH_4$ I. Crystal structure. *J. Alloys Compounds* **2002**, *346*, 200–205.

12. Hartman, M.R.; Rush, J.J.; Udovic, T.J.; Bowman, J.R.C.; Hwang, S.-J. Structure and vibrational dynamics of isotopically labeled lithium borohydride using neutron diffraction and spectroscopy. *J. Solid State Chem.* **2007**, *180*, 1298–1305.
13. Filinchuk, Y.; Chernysov, D.; Nevidomskyy, A.; Dimitriev, V. High-Pressure Polymorphism as a step toward destabilization of $LiBH_4$. *Angew. Chem. Int. Ed.* **2008**, *47*, 529–532.
14. Filinchuk, Y.; Chernysov, D.; Cerny, R. Lightest Borohydride Probed by Synchrotron X-ray Diffraction: Experiment Calls for a New Theoretical Revision. *J. Phys. Chem. C* **2008**, *112*, 10579–10584.
15. Hagemann, H.; Filinchuk, Y.; Chernyshov, D.; van Beek, W. Lattice anharmonicity and structural evolution of $LiBH_4$: an insight from Raman and X-ray diffraction experiments. *Phase Transit.* **2009**, *82*, 344–355.
16. Mosegaard, L.; Moller, B.; Jorgensen, J.-E.; Filinchuk, Y.; Cerenius, Y.; Hanson, J.C.; Dimasi, E.; Besenbacher, F.; Jensen, T.R. Reactivity of $LiBH_4$: In Situ Synchrotron Radiation Powder X-ray Diffraction Study. *J. Phys. Chem. C* **2008**, *112*, 1299–1303.
17. Yvon, K. Hydrogen in novel solid-state metal hydrides. *Z. Kristallogr.* **2003**, *218*, 108–116.
18. Mosegaard, L.; Moller, B.; Jorgensen, J.-E.; Bösenberg, U.; Dornheim, M.; Hanson, J.C.; Cerenius, Y.; Walker, G.; Jakobsen, H.J.; Besenbacher, F., *et al.* Intermediate phases observed during decomposition of $LiBH_4$. *J. Alloys Compounds* **2007**, *446–447*, 301–305.
19. Harvey, K.B.; McQuaker, N.R. Low Temperature Infrared and Raman Spectra of Lithium Borohydride. *Can. J. Chem.* **1971**, *49*, 3282–3286.
20. Gomes, S.; Hagemann, H.; Yvon, K. Lithium boro-hydride $LiBH_4$ II. Raman spectroscopy. *J. Alloys Compounds* **2002**, *346*, 206–210.
21. Hagemann, H.; Gomes, S.; Renaudin, G.; Yvon, K. Raman studies of reorientation motions of $[BH_4]^-$ anionsin alkali borohydrides. *J. Alloys Compounds* **2004**, *363*, 126–129.
22. Racu, A.-M.; Schoenes, J.; Lodziana, Z.; Borgschulte, A.; Zűttel, A. High-Resolution Raman Spectroscopy Study of Phonon Modes in $LiBH_4$ and $LiBD_4$. *J. Phys. Chem. A* **2008**, *112*, 9716–9722.
23. Talyzin, A.V.; Andersson, O.; Sundqvist, B.; Kurnosov, A.; Dubrovinsky, L. High-pressure phase transition in $LiBH_4$. *J. Solid State Chem.* **2007**, *180*, 510–517.
24. Corey, R.L.; Shane, D.T.; Bowman, R.C.; Conradi, M.S. Atomic Motions in $LiBH_4$ by NMR. *J. Phys. Chem. C* **2008**, *112*, 18706–18710.
25. Skripov, A.V.; Soloninin, A.V.; Filinchuk, Y.; Chernyshov, D. Nuclear Magnetic Resonance Study of the Rotational Motion and the Phase Transition in $LiBH_4$. *J. Phys. Chem. C* **2008**, *112*, 18701–18705.
26. Stasinevich, D.S.; Egorenko, G.A. Thermographic Investigation of Alkali Metal and Magnesium Tetrahydroborates and Pressures up to 10 atm. *Russ. J. Inorg. Chem.* **1968**, *13*, 341–343.
27. Orimo, S.; Nakamori, Y.; Zuttel, A. Material properties of MBH_4 (M = Li, Na, and K). *Mater. Sci. Eng. B* **2004**, *108*, 51–53.
28. Fedneva, E.M.; Alpatova, V.I.; Mikheeva, V.I. Thermal stability of lithium tetrahydroborate. *Russ. J. Inorg. Chem.* **1964**, *9*, 826–827.

29. Llewellyn, P.L.; Horcajada, P.; Maurin, G.; Devic, T.; Rosenbach, N.; Bourrelly, S.; Serre, C.; Vincent, D.; Loera-Serna, S.; Filinchuk, Y., *et al.* Complex Adsorption of Short Linear Alkanes in the Flexible Metal-Organic-Framework MIL-53(Fe). *J. Am. Chem. Soc.* **2009**, *131*, 13002–13008.
30. Hammersley, A.P.; Svensson, S.O.; Hanfland, M.; Fitch, A.N.; Häusermann, D. Two-dimensional detector software: From real detector to idealised image or two-theta scan. *High Pressure Res.* **1996**, *14*, 235–248.
31. Vogel, S.; Ehm, L.; Knorr, K.; Braun, G. Automated processing of 2D powder data. *Adv. X-ray Anal.* **2002**, *45*, 31–33.
32. Rodriguez-Carvajal, J. Recent advances in magnetic structure determination by neutron powder diffraction. *Physica B* **1993**, *192*, 55–69.
33. Kato, S.; Bielmann, M.; Borgschulte, A.; Zakaznova-Herzog, V.; Remhof, A.; Orimo, S.-i.; Zuttel, A. Effect of the surface oxidation of $LiBH_4$ on the hydrogen desorption mechanism. *Phys. Chem. Chem. Phys.* **2010**, *12*, 10950–10955.
34. Cahen, S.; Eymery, J.B.; Janot, R.; Tarascon, J.M. Improvement of the $LiBH_4$ hydrogen desorption by inclusion into mesoporous carbons. *J. Power Sources* **2009**, *189*, 902–908.
35. Dmitriev, V.; Filinchuk, Y.; Chernyshov, D.; Talyzin, A.V.; ilewski, A.; Andersson, O.; Sundqvist, B.; Kurnosov, A. Pressure-temperature phase diagram of $LiBH_4$: Synchrotron x-ray diffraction experiments and theoretical analysis. *Phys. Rev. B* **2008**, *77*, 174112.